# Reaction route and mechanism of the direct N-alkylation of sulfonamides on acidic mesoporous zeolite Beta catalyst

Wenqian Fu, Runsheng Shen, Enhui Bai, Lei Zhang, Qun Chen, Zhongxue
Fang, Guangchao Li, Xianfeng Yi, Anmin Zheng, and Tiandi Tang

### Just Accepted

# Reaction route and mechanism of the direct *N*-alkylation of sulfonamides on acidic mesoporous zeolite Beta catalyst

Wenqian Fu,[†] Runsheng Shen,[†] Enhui Bai,[†] Lei Zhang,[†] Qun Chen,*[†] Zhongxue Fang,[†] Guangchao Li,[‡] Xianfeng Yi,[‡] Anmin Zheng,*[‡] Tiandi Tang*[†]

[†]Jiangsu Key Laboratory of Advanced Catalytic Materials and Technology, School of Petrochemical Engineering, Changzhou University, Changzhou, Jiangsu 213164, P. R. China.

[‡]State Key Laboratory of Magnetic Resonance and Atomic and Molecular Physics, National Center for Magnetic Resonance in Wuhan, Key Laboratory of Magnetic Resonance in Biological Systems, Wuhan Institute of Physics and Mathematics, the Chinese Academy of Sciences, Wuhan 430071, P. R. China.

ABSTRACT: Development of highly active heterogeneous catalysts with strong acidity and mesoporous structure is a highly attractive strategy for organic synthesis. In this study, a mesoporous zeolite Beta (HBeta-M) with bulky particle size and strong acidity was synthesized and used in the direct *N*-alkylation of sulfonamides with alcohols. The strongly acidic HBeta-M had a higher intrinsic activity, with initial turnover frequency of $11\times10^{-2}$ $s^{-1}$, than H-form mordenite nanosheets ($3.3\times10^{-2}$ $s^{-1}$) and montmorillonite ($4.0\times10^{-2}$ $s^{-1}$) catalysts. The experiment and characterization results demonstrate that there are two parallel reaction routes on the acidic catalysts. One route is the reaction of benzhydrol with *p*-toluenesulfonamide (Route-I). Another route is the reaction of dibenzhydryl ether, arising from Route-I, with *p*-toluenesulfonamide (Route-II), which is found in this work. The reaction rate of Route-I ($13\times10^{-3}$ $mol\cdot kg^{-1}\cdot s^{-1}$) was higher than that of Route-II ($9.8\times10^{-3}$ $mol\cdot kg^{-1}\cdot s^{-1}$) on HBeta-M, but Route-II predominantly contributed to the formation of the target product with high selectivity. Hereby, a complete reaction mechanism was proposed in this work.

KEYWORDS: Mesoporous zeolite Beta, Strong acidity, *N*-alkylation, Reaction route, Reaction mechanism

## INTRODUCTION

The direct *N*-alkylation of amines with alcohols as the alkylation reagents is an important route for the construction of nitrogen-containing compounds, which are significant building blocks for pharmaceuticals and novel bio-active compounds.[1-3] Generally, this reaction requires suitable promoters due to the poor leaving ability of the hydroxyl group in alcohols,[4,5] leading to the formation of stoichiometric amounts of salt waste. Although other alkylating agents such as alkyl halides, sulfonates, aldehydes, diazomethane and carboxylic acid were replaced with alcohols for the *N*-alkylation of amines, by-products are inevitably formed during these reactions.[6-8] Alcohols, which are readily available, are still good alkylation reagents for *N*-alkylation reaction. To directly use alcohols as alkylation reagents while avoiding the waste formation, it is critical to develop highly efficient catalysts. With respect to this aspect, noble metal[9,10] and Lewis acid metal catalysts[11-13] have been developed for the direct substitution of alcohols with various nitrogen nucleophiles, such as amides, sulfonamides, carboxamides, carbamates, and amines. Among these protocols, a noble metal-catalyzed the *N*-alkylating sulfonamides with alcohols is an effective synthetic method using borrowing hydrogen methodology.[14] However, the high price of noble metal catalysts and the insufficient activity of Lewis acid metals limit their practical applications. Furthermore, the separation of products and metal salts from the reaction system is difficult and complicated, resulting in a tedious purification process and the formation of inevitable solid waste. These protocols not only did not meet the requirement of the green synthesis chemistry, but also was harmful to environmentally sustainable development. Solid catalysts, such as heteropoly acids,[15] proton-exchanged montmorillonite[16,17] and the acidic resin Amberlyst-15 in ionic liquid,[18] have also been employed for the amidation of alcohols. However, problems remain, including the dissolution of heteropoly acid, and the thermo- and chemical-

stability of the resins. The low surface area and the weak acidity of the montmorillonite also result in unsatisfactory activity in this transformation. On the other hand, it is notable that the proposed reaction mechanisms in the literatures are vague,[16,17,19] and have not been verified by experiment. Thus, developing highly efficient and green catalyst for the direct *N*-alkylation of amines with alcohols is critical. In addition, clarifying this reaction route and mechanism by experiment method is of significant importance.

Generally, acidic solid catalyst is able to cleave the carbon-oxygen bond of alcohols to produce carbocations through $H^+$ interaction with hydroxyl group in alcohols.[20] In the past decades, the mesoporous aluminosilicate zeolites as acidic catalysts show superior catalytic performance in many reactions.[21-23] In this respect, we synthesized a series of mesoporous zeolites and zeolite nanocrystal assemblies for applications in organic chemistry. [24-26] As part of our ongoing focus on the catalytic application of zeolite catalysts in organic synthesis, in this study, we report a facile method to synthesize mesoporous zeolite Beta (Beta-M) with large particle sizes at a large scale, which can be readily separated from the reaction mixture by simple filtration. After the Beta-M was ion-exchanged with a solution of $NH_4NO_3$ and calcined, the obtained H-form (HBeta-M) with strong acidity shows high activity in the direct *N*-alkylation of sulfonamides with benzylic alcohols, compared to the H-form of mordenite nanosheets (NS-HMOR), montmorillonite (HMont) and mesopore-free zeolite Beta (HBeta). Very importantly, this reaction on acidic HBeta-M proceeds through two parallel reaction routes. One route is adsorption and activation of benzylic alcohols on acidic sites, producing carbocation intermediates, which are attacked by the sulfonamide nucleophiles to form the *N*-substituted sulfonamide products (Route-I). The other route is the easy transformation of the benzylic

alcohols on the strongly acidic sites to ethers, which are more active towards the formation of carbocation intermediates, facilitating the formation of the target products (Route-II).

## 2 Experimental

### 2.1 Materials synthesis

A typical synthesis of mesoporous zeolite Beta was performed as follows. 0.34 kg NaOH was dissolved in 19 L $H_2O$ with stirring, followed by addition of 0.73 kg $NaAlO_2$ and 6 L 25 wt.% tetraethylammonium hydroxide (TPAOH). After stirring at room temperature for 1 h, 8.5 kg silica gel was added to the above solution and stirred for 1 h. A cationic copolymer (4.5 L) containing quaternary ammonium groups (RCC) was added dropwise and the mixture was stirred for 2 h to obtain a gel. The mesoscale template of RCC was synthesized as in our previous work.[27] The composition of this final gel was $Al_2O_3/32SiO_2/2Na_2O/0.01RCC/2.6TPAOH/296H_2O$. This gel was transferred into a 50 L autoclave for dynamic crystallization at 140 °C for 6 days. The solid product was collected by filtration, dried, and calcined at 550 °C for 6 h to remove the organic template. The mesopore-free zeolite Beta (Beta) was synthesized according to a previously reported method.[28]

For comparison, mordenite nanosheets (NS-MOR) was synthesized according to a previously reported method.[27] Montmorillonite (Mont) was purchased from Sinopharm Chemical Reagent Co., Ltd. The H-form of these samples was obtained by ion exchange with a 1 M $NH_4NO_3$ solution at 80 °C for 4 h, followed by calcination at 550 °C for 4 h. The solid catalysts were denoted as HBeta-M, NS-HMOR, HBeta and HMont, respectively.

### 2.2 Characterization

The X-ray powder diffraction (XRD) pattern was recorded on a D/MAX 2500/PC powder diffractometer (Rigaku) using a Cu $K\alpha$ radiation source operated at 40 kV and 200 mA. Nitrogen physisorption was conducted at -196 °C on a Micromeritics ASAP 2020M apparatus. The sample was degassed for 8 h at 300 °C before the measurement. The ratios of Si/Al in the zeolites were determined by inductively coupled plasma optical emission spectroscopy (ICP-OES) with a Perkin-Elmer 3300DV emission spectrometer. Scanning electron microscopy (SEM) was performed using a SUPRA 55 field emission scanning electron microscope operating at an acceleration voltage of 5 kV. Before the analysis, the sample was coated with gold to create contrast. Transmission electron microscopy (TEM) was performed on a JEM-2100F microscope with a limited line resolution capacity of 1.4 Å at 200 kV. Before characterization by TEM, the sample was cut into thin slices and dropped onto a Cu grid coated with a carbon membrane.

The acidity of the catalyst was measured by ammonia temperature-programmed desorption (NH$_3$-TPD) on a Micromeritics ASAP 2920 instrument. Typically, 200 mg of the sample was placed in a quartz tube and pretreated with a helium stream at 450 °C for 2 h. After the sample was cooled to 120 °C, an NH$_3$-He gas mixture (10 vol.% NH$_3$) was flowed over the sample for 30 min. After removing the physically adsorbed NH$_3$ by flowing helium for 2 h at 120 °C, the sample was heated from 120 to 520 °C at a rate of 10 °C·min$^{-1}$. The total acidic site density of the materials can be obtained from the total amount of the desorption ammonia, which was collected in dilute hydrochloric acid solution and then titrated with a dilute sodium hydroxide solution. Generally, the strength of the acidic sites is determined by desorption activation energy of the adsorbed ammonia, which is related to the desorption temperature of the adsorbed NH$_3$.[29,30] Based on the desorption temperature of the adsorbed NH$_3$, the acidic sites can be classified as weak acidic (120–250 °C), medium strong acidic (250–350°C), and strong acidic

(>350°C) sites.[31] Thus, the obtained $NH_3$-TPD curves were deconvoluted at different maximum peak temperatures with a Gaussian function for fitting,[32] and the peak areas were calculated. The peak areas were correlated with the amount of adsorbed $NH_3$ in different temperature regions. The acidity of the HBeta-M was also investigated by solid-state ^{31}P nuclear magnetic resonance (^{31}P NMR) on a Bruker Ascend-500 spectrometer. The pyridine and 2,6-di-*tert*-butylpyridine temperature programmed desorption (Py-TPD and 2,6-DTBPy-TPD) were performed on a Micromeritics ASAP 2920 instrument.

The infrared spectra (IR) of the benzhydrol, dibenzhydryl ether and benzhydrol- and dibenzhydryl ether-chemisorbed catalyst samples were obtained on a Bruker TENSOR 27 infrared spectrophotometer equipped with a reactor cell. Before measurement, the catalyst sample was evacuated to $10^{-2}$ Pa at 50 °C for 20 h. The spectrum was obtained in absorbance mode and was shown after subtraction of a background spectrum obtained on the corresponding pure catalyst sample at 50 °C under vacuum. For comparison, the spectra of benzhydrol and dibenzhydryl ether were also recorded at room temperature. The ultraviolet-visible diffuse reflection (UV-Vis DR) spectra of the benzhydrol (**1a**), dibenzhydryl ether (**4a**), and **1a**- and **4a**-chemisorbed on HBeta-M (HBeta-M-**1a** and HBeta-M-**4a**) and HMont (HMont-**1a** and HMont-**4a**) samples were obtained on a Shimadzu UV-3600 spectrometer. Before characterization, the HBeta-M-**1a**, HBeta-M-**4a**, HMont-**1a** and HMont-**4a** solid samples were evacuated to $10^{-2}$ Pa at 50 °C for 20 h and then cooled to room temperature.

**2.3 Activity test**

**2.3.1 Apparent activity of the catalyst**

Before the reaction, the powdered catalyst was calcined at 300 °C for 2 h in air to remove physically adsorbed water. The typical experimental procedure for the *N*-alkylation of *p*-toluenesulfonamide with benzhydrol was as follows: powdered catalyst (20 mg), benzhydrol **1a** (0.3 mmol), *p*-toluenesulfonamide **2a** (0.6 mmol), and 1,2-dichloroethane (DCE, 1.5 mL), with diphenylmethane (50 μL) as an internal standard, were placed in a sealed tube (10 mL) under $N_2$ atmosphere. The sealed tube was put in an oil bath when the reaction temperature of the oil reached 80 °C and maintained at 80 °C for 4 h. The reaction temperature and stirring rate in the sealed tube was controlled using an IKA stirrer (model of RTC BS025). When the reaction was finished, the sealed tube was removed from the oil bath. After the reaction mixture in the sealed tube was cooled to room temperature, the reaction mixture was centrifuged to obtain the liquid phase. The liquid products were analyzed using an Agilent 7890B GC equipped with a flame ionization detector. The conversion and product selectivity were calculated as follows.

$$\text{Benzhydrol conversion} = \frac{\text{Moles of carbon reacted benzhydrol}}{\text{Moles of carbon in initial benzhydrol}} \times 100$$

$$\text{Product i selectivity} = \frac{\text{Carbon moles in product i}}{\text{Sum of carbon moles in product i}} \times 100$$

The moles of carbon in the products and unreacted benzhydrol were also the same as the moles of carbon in the initial benzhydrol. The pure product was obtained by flash column chromatography on silica gel using petroleum ether (60-90 °C) and ethyl acetate as eluents.

**2.3.2 Intrinsic activity of the catalyst**

To investigate the intrinsic activity of the catalyst, additional experiments were performed in a 300 mL Parr4848 stainless autoclave (Figure S1) under the reaction conditions that excluded the

mass and heat transfer limitations. For this purpose, the powdered catalyst sample was pelleted

under a pressure of 7.5 MPa, crushed, and screened to different mesh particles, and then these

particles were calcined at 300 °C for 2 h in air to remove physically adsorbed water before the

reaction test. The experiment was carried out as followed: 0.1 g tableted catalyst, 7.5 mmol

benzhydrol **1a**, 15 mmol *p*-toluenesulfonamide **2a**, and 130 mL DCE as the solvent, with 1 mL

diphenylmethane as an internal standard, at a temperature of 80 °C in a $N_2$ atmosphere. In this

case, the initial reaction rate can be calculated as follows.[33]

$$r_{obs} = \frac{n}{W} \times \frac{dx}{dt}$$

where $r_{obs}$ is the initial reaction rate (mol·kg$^{-1}$·s$^{-1}$), $n$ is the initial amount of benzhydrol (mol), $x$

is the benzhydrol (or dibenzhydryl ether) conversion, $W$ is the catalyst mass (kg), and $t$ is the

reaction time (s), d$x$ is the differential of the benzhydrol (or dibenzhydryl ether) conversion.

In addition, because the micropore sizes in HBeta-M and NS-HMOR are much smaller than the

dimensions of the bulk reactants and products (Table S1), the *N*-alkylation reaction mainly

occurs on the acidic sites in the mesopores and on the outer surface of the zeolite catalysts. Thus,

the acidic sites in the mesopores are responsible for the *N*-alkylation reaction. In this case, the

initial turnover frequency (TOF, s$^{-1}$) should be calculated based on the acidic site density in the

mesopore, given by the following equation:

$$TOF_{ini} = \frac{r_{obs}}{M_T y}$$

$$TOF_{ini}^S = \frac{r_{obs}}{M_{T,S} y}$$

where $TOF_{ini}$ is calculated based on the total acidic site density in the mesopores, $TOF_{ini}^S$ is calculated based on the strongly acidic site density in the mesopores. $M_T$ is the total acidic site density (mol·kg$^{-1}$), $M_{T,S}$ is the strong acidic site density (mol·kg$^{-1}$), and $y$ is the mesoporous content in the sample, which is calculated from the ratio of the external surface area to the BET surface area. The $y$ value for the HBeta-M, NS-HMOR, HMont is 0.25, 0.18 and 1.0, respectively.

### 2.3.3 Catalyst recycle

The recycle experiment for the HBeta-M catalyst was performed in a 300 mL Parr4848 stainless autoclave. When the reaction was finished, the catalyst was separated from the reaction mixture by filtration and thoroughly washed with dichloromethane. After that, the sample was dried at 100 °C for 12 h and calcined at 550 °C for 4 h in air before use in the next cycle.

### 2.4. Benzhydrol and dibenzhydryl ether adsorption experiment

The adsorption experiment was carried out following: 0.2 g powdered catalyst, 40 mg of benzhydrol (or dibenzhydryl ether) and 65 μL diphenylmethane (as an internal standard) was dissolved in DCE (10 mL) in a 25 mL sealed tube with a magnetic stir bar. Then, the sealed tube was put in an oil bath at 60 °C for 3 h under stirring. After cooling to room temperature, the liquid phase was separated by filtration from the suspension and was analyzed using Agilent 7890B GC. The remaining solid sample was washed with DCE (15 mL) 20 times to eliminate the physically adsorbed benzhydrol (or dibenzhydryl ether) and dried at 60 °C for 48 h. The resulting solid sample was evacuated ($10^{-2}$ Pa) at 50 °C for 20 h and then used for UV-Vis DR spectrum and IR characterization as described above.

## 3 Results and discussion

### 3.1 Catalyst characterization

Figure 1a shows the powder XRD pattern of the Beta-M sample. The sample exhibits typical diffraction peaks at 7.7°, 21.4°, 22.6°, 25.4° and 27.1°, which are consistent with the Beta zeolite.[34] The nitrogen sorption isotherm of Beta-M exhibits a hysteresis loop at a relative pressure of 0.50-0.95, indicating the presence of mesoporous structure in the Beta-M (Figure 1b). The pore size distribution shows that the mesoporous diameter is mainly centered at 11 nm (inset, Figure 1b). The detailed textural parameters of the samples are given in Table 1. HBeta-M shows a high BET surface area (590 $m^2 \cdot g^{-1}$), mesoporous surface area (180 $m^2 \cdot g^{-1}$) and mesoporous volume (0.27 $cm^3 \cdot g^{-1}$). In contrast, the mesopore-free HBeta zeolite only has an external surface area of 58 $m^2 \cdot g^{-1}$ (Figure S2 and Figure S3, Table 1).
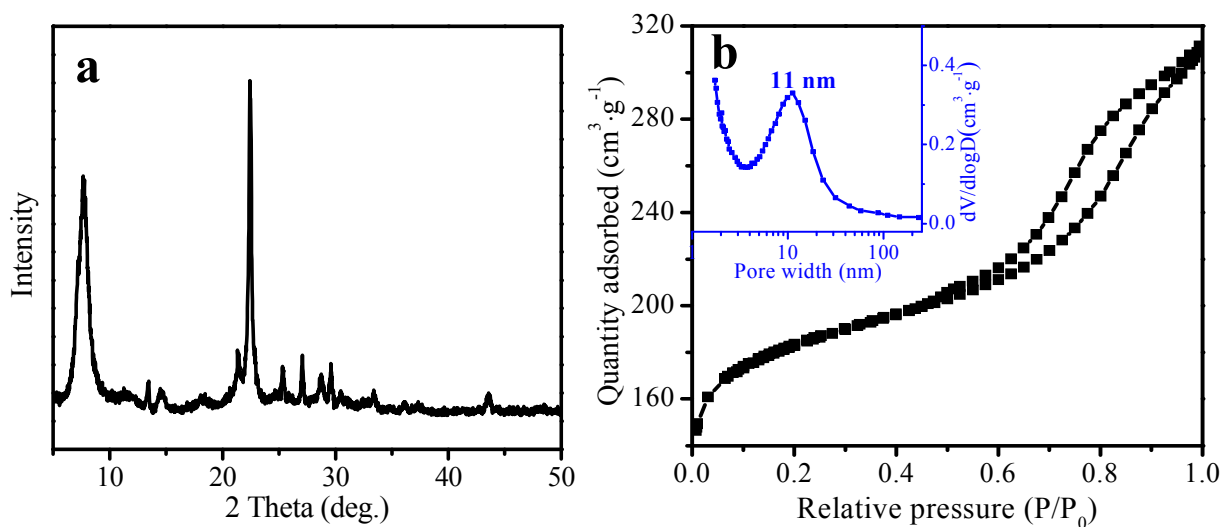


**Figure 1.** (a) XRD pattern and (b) $N_2$ adsorption isotherms of the Beta-M sample (inset, mesoporous size distribution).

Table 1 Textural parameters of the various catalysts.

| Samples | $S_{BET}$[a] $(m^2 \cdot g^{-1})$ | $V_{mic.}$[b] $(cm^3 \cdot g^{-1})$ | $S_{ext.}$[c] $(m^2 \cdot g^{-1})$ | $V_{mes.}$[d] $(cm^3 \cdot g^{-1})$ |
|---|---|---|---|---|
| HBeta-M | 590 | 0.16 | 180 | 0.27 |
| HBeta | 454 | 0.15 | 58 | 0.07 |
| HBeta-M[e] | 499 | 0.15 | 128 | 0.21 |
| NS-HMOR[e] | 474 | 0.15 | 86 | 0.19 |
| HMont[e] | 72 | 0.01 | 72 | 0.14 |
| Reused HBeta-M | 486 | 0.14 | 121 | 0.20 |

[a]BET surface area. [b]Microporous volume. [c]External surface area, including mesoporous surface area. [d]Mesoporous volume. [e]The sample was tableted under the pressure of 7.5 MPa before $N_2$-physisorption.

The SEM image reveals the Beta-M crystal particles with size of approximately 1 μm (Figure 2a), which is of significant importance in order to obtain products from the reaction mixture through separation by simple filtration method. The light areas in the TEM image of the thin-sectioned sample represent mesopore cavities within the crystals (Figure 2b). The size range of the mesopores, as determined by TEM analysis, is 7-12 nm, which is in agreement with the pore size distribution derived from the $N_2$ sorption experiments (inset in Figure 1b). These disordered mesopores are interconnected with ordered micropores. The morphology and the pore structure of NS-MOR and Mont were also investigated by SEM and TEM techniques and the results are shown in Figure S4 and Figure S5. It is clearly that the NS-MOR assemblies with a flower-shaped morphology have abundant interstitial meso- and macro-porous, and these nanosheets are highly crystalline (Figure S4).The SEM and TEM images of the Mont show that mangy fibers are present on the surface of the bulky Mont particles (Figure S5).
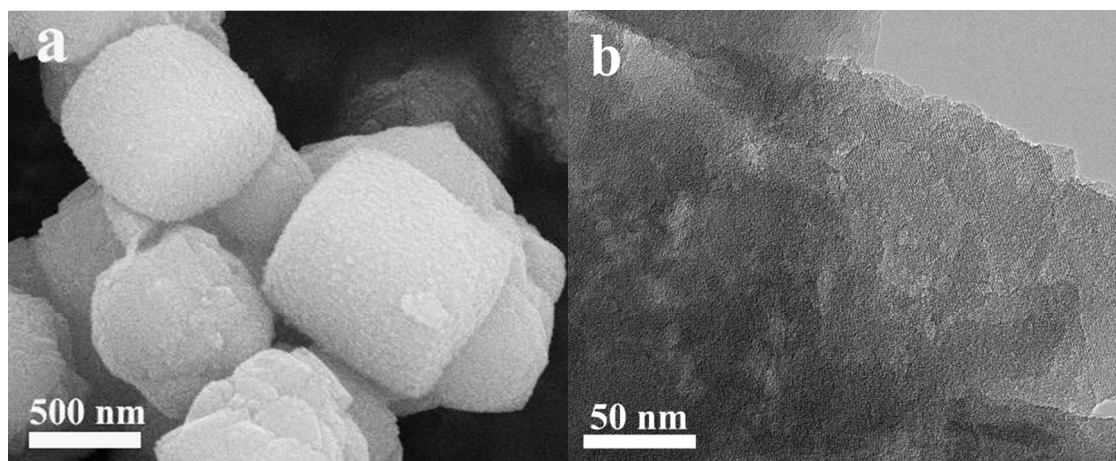
**Figure 2.** (a) SEM image of the Beta-M sample and (b) TEM image of the sliced Beta-M sample.

Figure 3 shows the $NH_3$-TPD curves of the three catalysts. The total acidic density, which was obtained by acid-base titration, is given in Table 2. It is clear that NS-HMOR has more weak acid sites than HBeta-M and HMont (Figure 3a and Figure 3b), and the total acidic density of NS-HMOR is 607 $\mu mol \cdot g^{-1}$, much higher than that of HBeta-M (461 $\mu mol \cdot g^{-1}$) and HMont (109 $\mu mol \cdot g^{-1}$, Table 2). Nevertheless, the relative areas of the deconvoluted peaks in the $NH_3$-TPD curves (Figure 3a) show that the medium acid sites density, and especially the strong acid site density of HBeta-M is much higher than that of NS-HMOR. Among these catalysts, HMont shows the lowest acidity (Figure 3b). The used HBeta-M shows similar $NH_3$ desorption curves compared to fresh HBeta-M (Figure S6). The acid site density of the used HBeta-M catalyst is 456 $\mu mol \cdot g^{-1}$, lower than that of HBeta (923 $\mu mol \cdot g^{-1}$, Table 2, Figure S7). This is due to that HBeta has a low ratio of Si/Al (Table 2).

The external and internal acid sites of the HBeta-M catalyst were examined by $^{31}P$ NMR spectra using phosphorus probe molecules with different kinetic diameter (KD) such as trimethylphosphine oxide (TMPO, KD=0.55 nm) and tributylphosphine oxide (TBPO, KD=0.82 nm). From Figure 4, two intense resonances at 69.1 and 63.8 ppm were observed for the TMPO

adsorbed on HBeta-M. The signal at 69.1 ppm was attributed to the TMPO interaction with relatively strong acid sites in HBeta-M sample.[35] The signal at 63.8 ppm was attributed to the TMPO interaction with relatively weak acid sites in HBeta-M sample.[35] This result indicates the presence of abundant acid sites with different acidic strengths in HBeta-M sample. For the TBPO adsorbed on HBeta-M (Figure 4a), multiple $^{31}$P peaks were observable. The peak at 57.3 ppm can be ascribed to physically adsorbed TBPO.[35] The broad peak at 73.7 ppm, based on the previous work,[35,36] corresponds to the 63.8-69.1 ppm for TMPO, which indicates that the external acidic sites have comparable acidic strength with the acidic sites in the micropore channels. The resonances at 84.4 and 92.3 ppm may be caused by the confinement effect imposed by the relative pore in the wall of larger channels in HBeta-M,[35] and such pore is much larger than the size of TMPO, but match well with the molecule size of TBPO, which lead to the formation of relatively strong acidic sites in the mesopores. Furthermore, this type of pore could act as an effective passageway that connects 12-MR and mesopores, which could benefit the reactant diffusion. In addition, alkyl ammonium temperature programmed desorption (TPD) experiments were also performed by choosing Py (KD=0.54 nm) and 2,6-DTBPy (KD=1.05 nm) as probe molecules.[37] From the Py-TPD and 2,6-DTBPy-TPD curves (Figure S8), it was found that there are present abundant internal and external acidic sites in the HBeta-M. Notably, both of the TPD curves show the desorption signal mainly centered at 211 °C, indicating that the acidic sites in the mesopores or on the outer surface have comparable acid strength to the internal acidic sites. It seems that the number of the internal acidic sites is higher than that of the external acidic sites according to the area of desorption profile. However, because the thermal conductivity of the Py and 2,6-DTBPy is different, the quantitative comparison of the internal and external acidic site density based on desorption curves area is unreasonable. Therefore, the

$^{31}$P NMR and Py-TPD (or 2,6-DTBPy-TPD) experimental results clearly illustrate the presence

of abundant accessible acid sites in the mesoporous for the bulky reactants in HBeta-M catalyst.
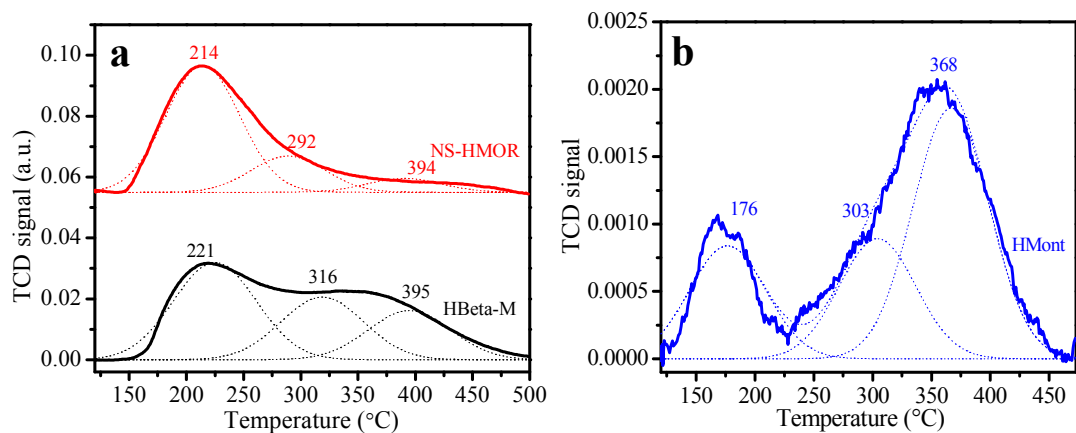


**Figure 3.** NH$_3$-TPD curves and Gaussian deconvoluted peaks for the (a) HBeta-M, NS-HMOR
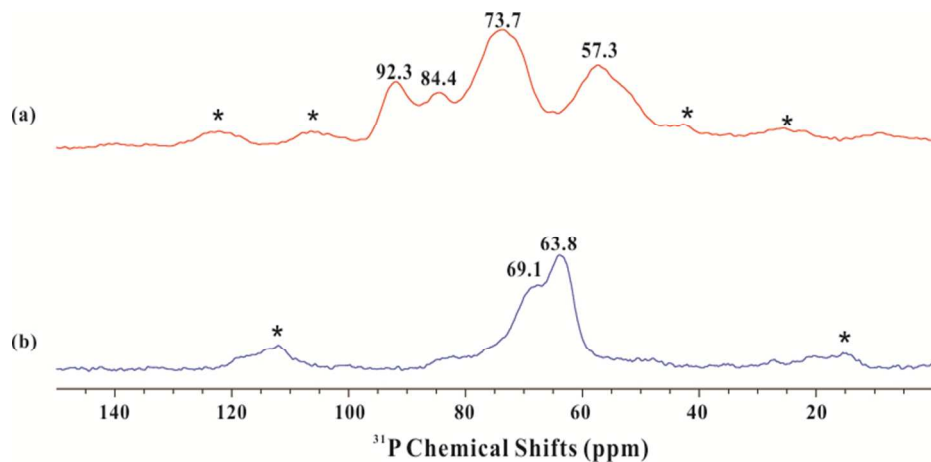
and (b) HMont samples.



**Figure 4.** $^{31}$P NMR spectra of (a) TBPO and (b) TMPO adsorbed on HBeta-M zeolite. The

sample spinning rate is 10 kHz. * denotes spinning sidebands.

**Table 2.** Total acidity and acidic site distribution of the catalysts.

| Catalyst | Weak acid sites ($\mu$mol·g$^{-1}$)$^a$ | Medium acid sites ($\mu$mol·g$^{-1}$)$^a$ | Strong acid sites ($\mu$mol·g$^{-1}$)$^a$ | Total acid sites ($\mu$mol·g$^{-1}$)$^b$ | Si/Al$^c$ |
|---|---|---|---|---|---|

| HBeta-M | 212 | 139 | 110 | 461 | 16 |
| NS-HMOR | 429 | 127 | 51 | 607 | 8 |
| HMont | 26 | 26 | 57 | 109 | - |
| HBeta | 498 | 303 | 122 | 923 | 7 |

[a]Weak acid sites, Medium acid sites, Strong acid sites estimated from the relative area of the deconvoluted peak, respectively. [b] Total acid site determined by titration technique. [c] The Si/Al ratios determined by ICP.

## 3.2 External and internal mass transfer limitations

To compare the intrinsic activity of the catalysts for the *N*-alkylation reaction, the mass transfer limitation was excluded experimentally and theoretically. The external mass transfer limitation in a batch reactor was investigated through changing the stirring rate[33] for the *N*-alkylation of *p*-toluenesulfonamide with the HBeta-M, NS-HMOR and HMont catalysts. Figure S9 shows the benzhydrol conversion versus stirring rate. The benzhydrol conversion on the HBeta-M catalyst increased linearly with increasing stirring rate when the stirring rate was less than 150 rpm and remained almost constant after the stirring rate exceeded 150 rpm. A similar phenomenon was also observed on the NS-HMOR and HMont catalysts. These results indicate that the external mass transfer limitation could be excluded under stirring speed of 150 rpm. Hence, in the following studies, 500 rpm was used for the *N*-alkylation of *p*-toluenesulfonamide with benzhydrol.

In addition, a Weisz–Prater analysis was performed.[38,39] The Weisz–Prater criterion with the HBeta-M catalyst gave $C_{WP} = \frac{r_{obs}\rho_c R_p^2}{D_{eff}C_s} = 4.7 \times 10^{-4} < 1$. Similarly, the Weisz–Prater criterion with the

NS-HMOR and HMont catalysts was also less than 1, indicating no internal diffusion limitations (please see the Supporting Information for details).[38,39] On the other hand, we also investigated the effect of the HBeta-M particle size on the reaction rate under different reaction temperatures to further confirm the elimination of internal mass transfer limitation according to previously reported study.[40] The results are shown in Table 3. At 80 °C, the $r_{obs}$ for HBeta-M remains almost unchanged when the particle size is less than 120 μm, indicating that the internal mass transfer limitation could be eliminated for the HBeta-M catalyst with a particle size of less than 120 μm. Furthermore, when the temperature was reduced to 70 °C, the $r_{obs}$ for HBeta-M with a particle size of 109-120 μm is similar to that of relatively small particle HBeta-M (<109 μm), indicating that the activity at 70 and 80 °C is independent of particle size. These results further demonstrate that the catalytic activity are free from the effect of internal mass transfer at 80 °C on the HBeta-M catalyst with a particle size of 109-120 μm and a stirring speed of 500 rpm. Considering that this reaction mixture contains 130 mL 1,2-chloroethane and little benzhydrol **1a** (7.5 mmol) and *p*-toluenesulfonamide **2a** (15 mmol), the effect of the heat transfer limitation on the reaction activity may be negligible (please see the Supporting Information for details).

**Table 3.** Activity for different sized particles of HBeta-M catalyst in the *N*-alkylation of p-toluenesulfonamide with dibenzhydrol.[a]

| Particle size | $r_{obs,1}$ ($\times 10^{-2}$ mol·kg$^{-1}$·s$^{-1}$) | |
|---|---|---|
| | 80 °C | 70 °C |
| 100-120 (120-150 μm) | 0.7 | - |
| 120-140 (109-120 μm) | 1.3 | 0.33 |
| >140 (<109 μm) | 1.3 | 0.34 |

[a]Reaction conditions: 0.1 g HBeta-M catalyst, 7.5 mmol **1a**, 15 mmol **2a**, 130 mL DCE as solvent, 1 mL diphenylmethane.

### 3.3 Catalyst performance and the reaction route

### 3.3.1 Apparent activity of the catalyst

Under the catalytic reaction system in 10 mL tubule, the *N*-alkylation of *p*-toluenesulfonamide with benzhydrol produced the desired product **3a**, *N*-substituted sulfonamide, and a side product, dibenzhydryl ether **4a** (Table 4). Notably, the conversion of benzhydrol on the HBeta-M catalyst (98%) is higher than that on the NS-HMOR (89%), HBeta (12%) and HMont (42%) catalysts. The Cu(OAc)$_2$ salt gives a very low benzhydrol conversion of 1.3%. In particular, HBeta-M shows the highest target product selectivity (96%), as compared to the NS-HMOR (52%), HBeta (74%) and HMont (21%) catalysts.

**Table 4.** The *N*-alkylation of p-toluenesulfonamide with benzhydrol over different catalysts.[a]
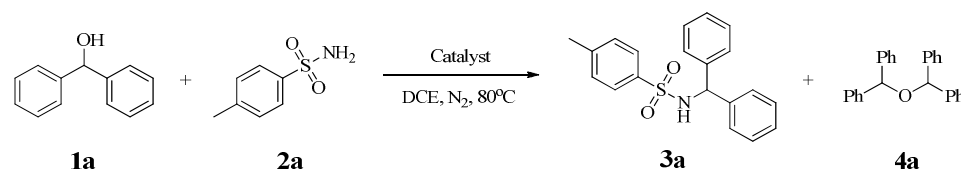


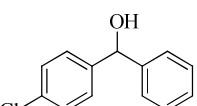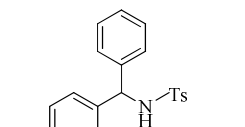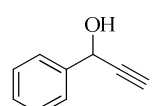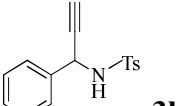| Entry | Catalyst | Conversion (%)[b] | Selectivity[b] (%) | |
|---|---|---|---|---|
| | | | Product **3a** | Dibenzhydryl ether **4a** |
| 1 | HBeta-M | 98 | 96 | 4 |
| 2 | NS-HMOR | 89 | 52 | 48 |
| 3 | HMont | 42 | 21 | 79 |
| 4 | Cu(OAc)$_2$[c] | 1.3 | 55 | 45 |
| 5 | HBeta | 12 | 74 | 26 |
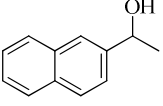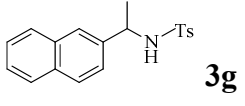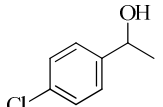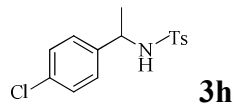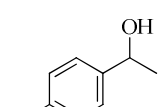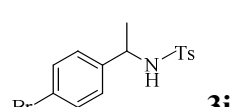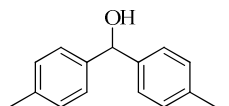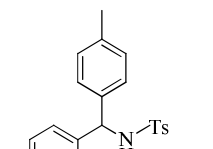
In addition, the reaction substrate scope on the HBeta-M catalyst was also investigated and the results are shown in Table 5, Table 6 and Table S2. At first, the *N*-alkylation of *p*-toluenesulfonamide was examined using a series of aromatic alcohols (Table 5). The HBeta-M catalyst tolerated various α-methyl phenylcarbinols with different electron-donating groups (*p-n*-butyl, *o*-methoxyl, *p*-methylmercapto and so on) and electron-withdrawing groups (chlorine and bromine), affording the corresponding *N*-substituted sulfonamides **3b-3i** in high yields (92-100%). In addition, the HBeta-M catalyst was used in the substitution of benzhydrol with methyl and bromine groups, also giving the corresponding products (**3j** and **3k**) in good yields (100 and 96%). Furthermore, when the relatively inactive 1-phenyl-2-propyne alcohol was used as a substrate, the HBeta-M catalyst afforded good catalytic performance, giving the product with a yield of 72% (**3l**).

Secondly, the generality of the *N*-alkylation of various amides with benzhydrol on the HBeta-M catalyst was tested (Table 6). The substitution of benzhydrol by a series of benzsulfamides (containing electron-donating or electron-withdrawing groups) using the HBeta-M catalyst proceeded smoothly, delivering the desired products (**3m-3q**) in good yields (91-100%). When inactive amides, such as *p*-toluamide and acrylamide were used as substrates, the desired products (**3r** and **3s**) were obtained in moderate yields using HBeta catalyst (73 and 68%) when the reaction temperature was raised to 100 °C for 20 h. This could be due to that the *p*-toluamide can be transformed to 4-methylbenzimidic acid, and acrylamide can be transformed to acrylimidic acid under reaction conditions (Scheme S1)[41], resulting in the reduction of the

nucleophilicity of the amides. In addition, the generality of the HBeta-M catalyst in this *N*-alkylation was further investigated through choosing primary benzyl alcohols and alkyl alcohols as alkylation reagent. The benzyl alcohol, isoamyl alcohol and cyclopentanol were suitable for this transformation, giving the desired products in good to high yields (Table S2). These results indicate that HBeta-M has good substrate tolerance.
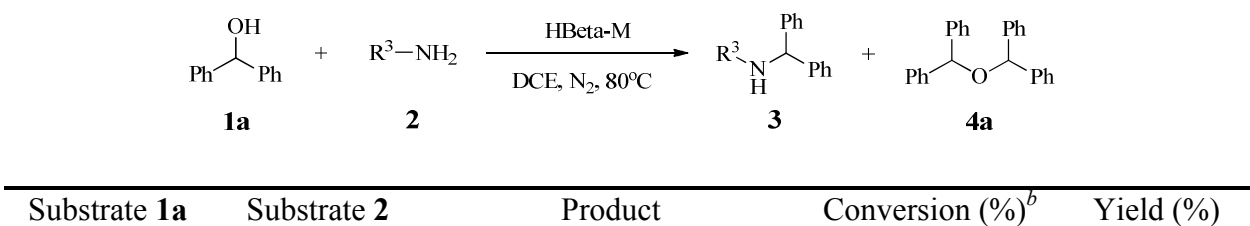
**Table 5.** The *N*-alkylation of *p*-toluenesulfonamide with a series of alcohols on the HBeta-M catalyst.[a]
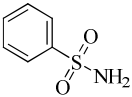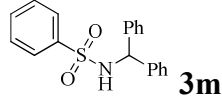


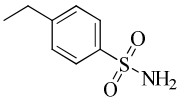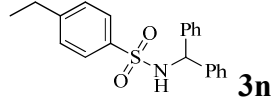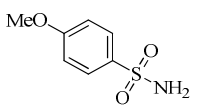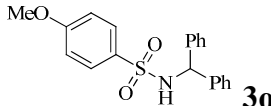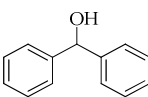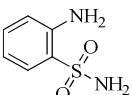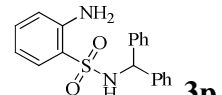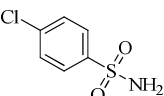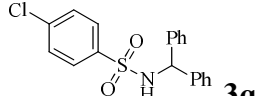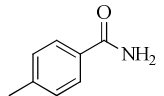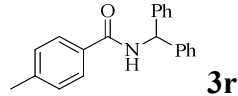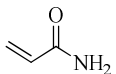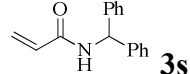| Substrate **1** | Substrate **2a** | Product[b] | Conversion (%)[c] | Yield (%) |
|---|---|---|---|---|
|  | |  **3b** | 100 | 99 |
|  | |  **3c** | 100 | 100 |
|  |  |  **3d** | 100 | 100 |
|  | |  **3e** | 100 | 98 |
|  | |  **3f** | 100 | 99 |

**3g** 98 93

**3h** 100 92

**3i** 100 90

**3j** 100 100

**3k** 100 96

**3l** 83 72

[a]Reaction conditions: catalyst (20 mg), substrate **1** (0.3 mmol), substrate **2a** (0.6 mmol), DCE (1.5 mL) as solvent, 80 °C for 6 h. [b]Ts = p-toluenesulfonyl. [c]The reaction mixture was analyzed by GC.

**Table 6.** The N-alkylation of series of amides with benzhydrol on the HBeta-M catalyst.[a]

$$Ph\text{-}CH(OH)\text{-}Ph \quad \mathbf{1a} \quad + \quad R^3\text{-}NH_2 \quad \mathbf{2} \quad \xrightarrow[\text{DCE, N}_2, 80°C]{\text{HBeta-M}} \quad R^3\text{-}NH\text{-}CH(Ph)\text{-}Ph \quad \mathbf{3} \quad + \quad Ph\text{-}CH(Ph)\text{-}O\text{-}CH(Ph)\text{-}Ph \quad \mathbf{4a}$$

| Substrate **1a** | Substrate **2** | Product | Conversion (%)[b] | Yield (%) |
|---|---|---|---|---|

| | | | |
|---|---|---|---|
| | phenyl sulfonamide | **3m** | 100 | 100 |



| | | | |
|---|---|---|---|
| | | **3m** | 100 | 100 |
| | | **3n** | 98 | 91 |
| | | **3o** | 99 | 95 |
| | | **3p** | 100 | ~100 |
| | | **3q** | 100 | 92 |
| | | **3r** | 88[c] | 73 |
| | | **3s** | 81[c] | 68 |

[a]Reaction conditions: catalyst (20 mg), substrate **1a** (0.3 mmol), substrate **2** (0.6 mmol), DCE (1.5 mL) as solvent, 80 °C for 6 h. [b]The reaction mixture was analyzed by GC. [c]The reaction temperature is 100 °C and the reaction time is 20 h.

### 3.3.2 Two reaction routes

Generally, the *N*-alkylation of sulfonamides with alcohols mainly proceeds on the Brönsted acid sites. The benzylic alcohol interacted with the acid site (H⁺) and is protonated by H⁺ to give an oxonium ion. This oxonium ion is dehydrated to form a carbocation intermediate, which is attacked by the electric-rich nucleophile of the sulphonamide. The subsequent deprotonation generates the desired *N*-substituted sulfonamide.[15,17] However, in this work, not only was the

desired product of *N*-benzhydryl-4-methylbenzenesulfonamide **3a** formed, but a by-product, dibenzhydryl ether **4a**, was also observed when the reaction was conducted in a sealed tube (10 mL) or in a 300 mL Parr autoclave where mass transfer was excluded (Table 3 and Table 7). It is particularly noteworthy that when the by-product dibenzhydryl ether **4a** was used as starting substrate, the *N*-alkylation of *p*-toluenesulfonamide **2a** with **4a** over the three catalysts also proceeded smoothly in the 300 mL Parr autoclave (Table 8). It is found that, at a reaction time of 9 h, the product **3a** was obtained with high selectivity over the HBeta-M (98%) and NS-HMOR (94%) catalysts in the *N*-alkylation of sulfonamides with dibenzhydryl ether **4a** (Table 8), as compared to the *N*-alkylation of *p*-toluenesulfonamide **2a** with benzhydrol **1a** (90% for HBeta-M and 67% for NS-HMOR, Table 7). These results indicate that there could be two reaction routes yielding the target product **3a** in the *N*-alkylation of sulfonamides on acidic catalysts (Figure 5). One route is the reaction of benzhydrol **1a** with *p*-toluenesulfonamide **2a**, here called Route-I, which is in agreement with the reported literatures.[15,17] The other route is the reaction of the by-product dibenzhydryl ether **4a**, that could be transformed from benzhydrol **1a,** with *p*-toluenesulfonamide **2a**. This reaction route is not reported in previous researches, here named Route-II in this work.

**Table 7.** The product distribution in the *N*-alkylation of *p*-toluenesulfonamide with benzhydrol over different catalysts at reaction time of 9 h.[a]



| Catalyst | Benzhydrol Conversion (%)[b] | Selectivity (%)[b] | |
|---|---|---|---|
| | | Product **3a** | Dibenzhydryl ether **4a** |

| | | | |
|---|---|---|---|
| HBeta-M | 89 | 90 | 10 |
| NS-HMOR | 81 | 67 | 33 |
| HMont | 56 | 50 | 50 |

[a]Reaction conditions: 0.1 g catalyst (120-140 mesh), 7.5 mmol benzhydrol **1a**, 15 mmol *p*-toluenesulfonamide **2a**, 130 mL DCE, 1.0 mL diphenylmethane, 80 °C, 500 rpm. [b]Conversion and selectivity are obtained from GC data.

**Table 8.** The product distribution in the *N*-alkylation of *p*-toluenesulfonamide with dibenzhydryl ether over different catalysts at reaction time of 9 h.[a]
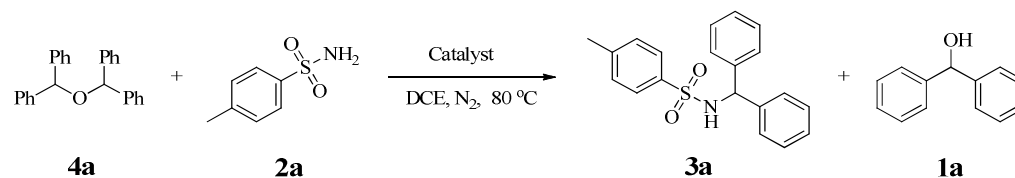


| Catalyst | Dibenzhydryl ether Conversion (%)[b] | Selectivity (%)[b] | |
|---|---|---|---|
| | | Product **3a** | Benzhydrol 1**a** |
| HBeta-M | 100 | 98 | 2 |
| NS-HMOR | 96 | 94 | 6 |
| HMont | 59 | 65 | 35 |

[a]Reaction conditions: 0.1 g catalyst (120-140 mesh), 3.75 mmol dibenzhydryl ether **4a**, 15 mmol *p*-toluenesulfonamide **2a**, 130 mL DCE, 1.0 mL diphenylmethane, 80 °C, 500 rpm. [b]Conversion and selectivity are obtained from GC data.
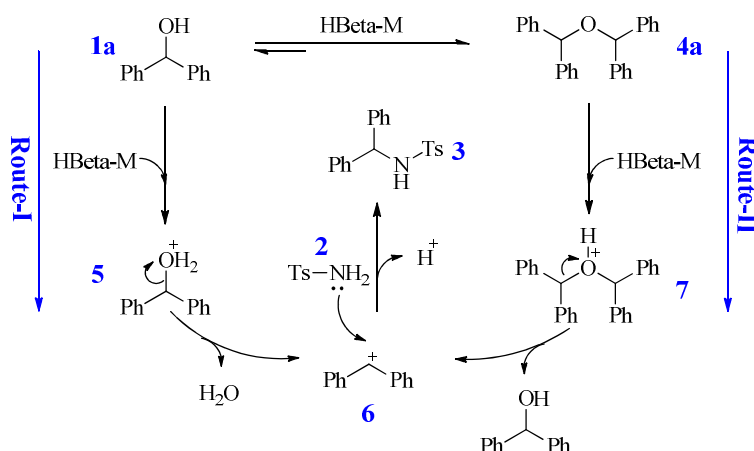
**Figure 5.** The reaction route for the *N*-alkylation of sulfonamides with benzylic alcohols.

To verify whether the benzhydrol **1a** could be transformed to dibenzhydryl ether **4a**, the experiments for the conversion of benzhydrol **1a** to dibenzhydryl ether **4a** (**1a→4a**) and vice versa (**4a→1a**) were carried out under the same reaction conditions in the 300 mL autoclave in the absence of mass transfer limitations on the HBeta-M, NS-HMOR and HMont catalysts. Obviously, **1a** was quickly converted to **4a** in the **1a→4a** reaction (Figure 6a); in contrast, the transformation from **4a** to **1a** was relatively difficult in the **4a→1a** reaction (Figure 7a). For clarity, the reaction rate of this reversible reaction was calculated. As expected, the reaction rates $r_{obs,3}$ of **1a→4a** are much higher than the reaction rates $r_{obs,4}$ of **4a→1a** on the three catalysts (Figure 6b and Figure 7b). For example, the $r_{obs,3}$ of **1a→4a** ($46\times10^{-3}$ mol·kg$^{-1}$·s$^{-1}$, Figure 6b) is much higher than the $r_{obs,4}$ of **4a→1a** ($3.4\times10^{-3}$ mol·kg$^{-1}$·s$^{-1}$, Figure 7b) on the HBeta-M catalyst. In addition, it is notable that not only $r_{obs,3}$ (**1a→4a**) but also $r_{obs,4}$ (**4a→1a**) of HBeta-M ($46\times10^{-3}$ and $3.4\times10^{-3}$ mol·kg$^{-1}$·s$^{-1}$) are higher than those of NS-HMOR ($26\times10^{-3}$ and and $3.1\times10^{-3}$ mol·kg$^{-1}$·s$^{-1}$) and HMont ($20\times10^{-3}$ and $2.1\times10^{-3}$ mol·kg$^{-1}$·s$^{-1}$), which suggests that benzhydrol **1a** is more readily converted to dibenzhydryl ether **4a** on HBeta-M. These results indicated that the **1a** was

easily transformed to **4a**, which can readily react with **2a**, enhancing the reaction selectivity on the acidic catalysts, especially on the strong acidic HBeta-M catalyst.



**Figure 6.** (a) Benzhydrol **1a** conversion versus reaction time, and (b) kinetics analysis for the transformation of benzhydrol **1a** to dibenzhydryl ether **4a** using different catalysts (reaction conditions: 0.1 g 120-140 mesh catalyst, 7.5 mmol benzhydrol **1a**, 130 mL DCE, 1 mL diphenylmethane, 80 °C, 500 rpm).
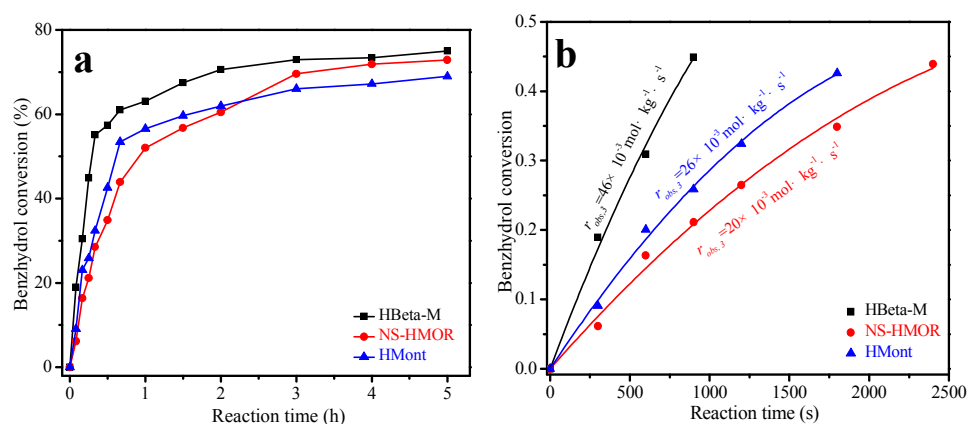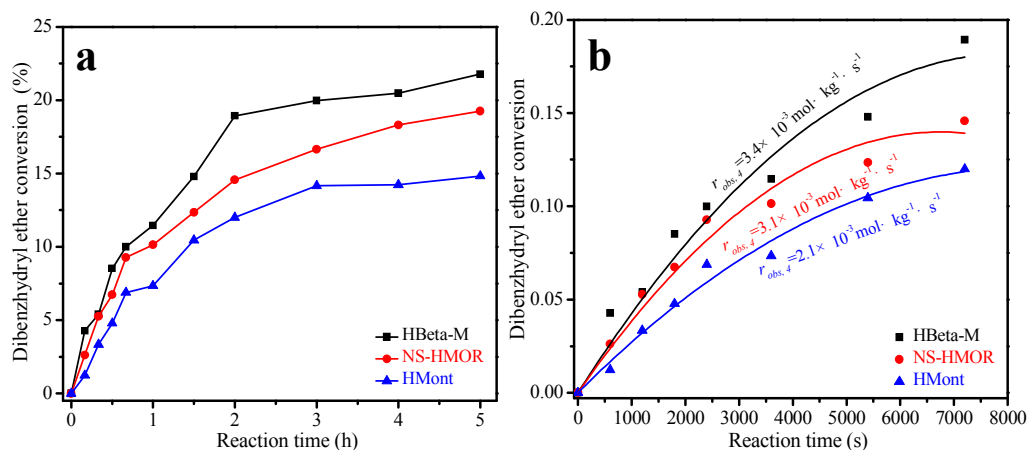


**Figure 7.** (a) Dibenzhydryl ether **4a** conversion versus reaction time, and (b) kinetics analysis for the transformation of dibenzhydryl ether **4a** to benzhydrol **1a** using different catalysts (reaction conditions: 0.1 g 120-140 mesh catalyst, 3.75 mmol dibenzhydryl ether **4a**, 130 mL DCE, 1 mL diphenylmethane, 80 °C, 500 rpm).

### 3.3.3 Comparison of the intrinsic activity on the two reaction routes

To compare the reaction activity aroused from the reaction Route I and Route II, the *N*-alkylation of *p*-toluenesulfonamide **2a** with benzhydrol **1a** and the *N*-alkylation of **2a** with dibenzhydryl ether **4a** were performed in a 300 mL Parr autoclave in the absence of mass transfer limitations. Clearly, the benzhydrol **1a** conversion on the HBeta-M catalyst is higher than that on NS-HMOR and HMont catalysts in the same reaction periods (Figure 8a). The product selectivity on the HBeta-M catalyst also rapidly increases with reaction time, but this phenomenon is not observed on the NS-HMOR and HMont catalysts (Figure 8b). It is notable that, comparing the Figure 8a and Figure 9a, although the **1a** conversion is higher than **4a** conversion at the same reaction time, the target product **3a** selectivity generated from Route-II is much higher than that from Route-I (Figure 8b and 9b). For example, the product **3a** selectivity on the HBeta-M catalyst is 96% from Route-II at 7 h, higher than that obtained from Route-I (86% at 7 h). For the HMont and NS-HMOR catalysts, the product **3a** selectivity in Route-II is also higher than those in Route-I. These results indicate that Route-II predominantly contributes to the formation of the product **3a** in the *N*-alkylation of sulfonamides over the three catalysts.
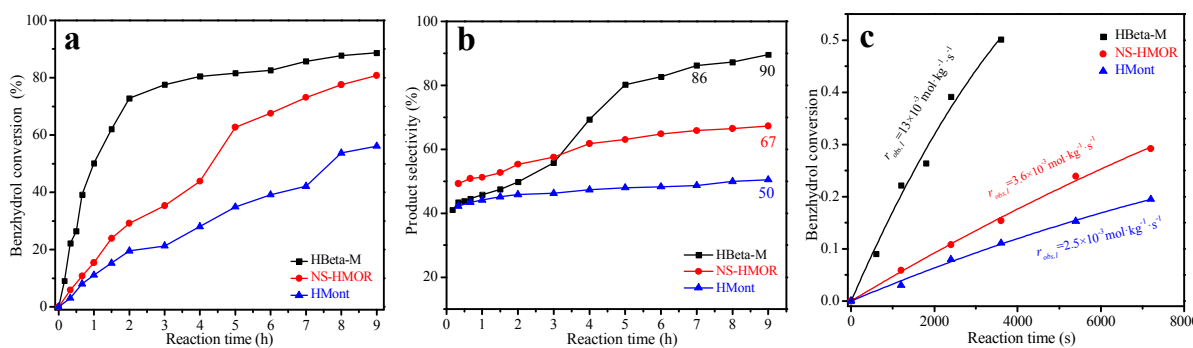


**Figure 8.** Dependence of (a) benzhydrol conversion, (b) product **3a** selectivity and (c) kinetics analysis on the reaction time in the *N*-alkylation of *p*-toluenesulfonamide with benzhydrol.
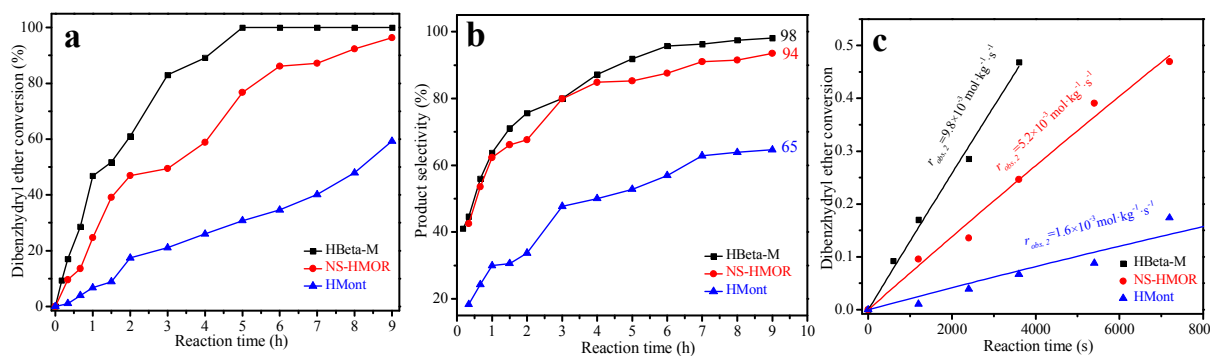
**Figure 9.** Dependence of (a) dibenzhydryl ether conversion, (b) product **3a** selectivity and (c) kinetics analysis on the reaction time in the *N*-alkylation of *p*-toluenesulfonamide with dibenzhydryl ether.

To better compare the reaction activity in Route-I and Route-II, the initial reaction rate ($r_{obs}$) was calculated and the results are shown in Figure 8c and Figure 9c. Clearly, $r_{obs,1}$ ($13 \times 10^{-3}$ mol·kg$^{-1}$·s$^{-1}$) for Route-I on the HBeta-M catalyst is higher than $r_{obs,2}$ ($9.8 \times 10^{-3}$ mol·kg$^{-1}$·s$^{-1}$) for Route-II. A similar phenomenon is observed on HMont catalyst. These results suggest that benzhydrol **1a** may easily be transformed to dibenzhydryl ether **4a** on the acidic catalyst and subsequently reacts with *p*-toluenesulfonamides **2a**. Thus, the reaction Route-II may be responsible for the formation of **3a** in high yield. On the other hand, from Figure 8c and Figure 9c, $r_{obs,1}$ and $r_{obs,2}$ on the HBeta-M ($13 \times 10^{-3}$ and $9.8 \times 10^{-3}$ mol·kg$^{-1}$·s$^{-1}$) are much higher than those on the NS-HMOR ($3.6 \times 10^{-3}$ and $5.2 \times 10^{-3}$ mol·kg$^{-1}$·s$^{-1}$) and HMont ($2.5 \times 10^{-3}$ and $1.6 \times 10^{-3}$ mol·kg$^{-1}$·s$^{-1}$), indicating that the HBeta-M catalyst is more active in the *N*-alkylation of sulfonamides with benzhydrol **1a** and with dibenzhydryl ether **4a**. The initial turnover frequencies (TOF, s$^{-1}$) were also determined based on the acid site density in the mesopore, and the results are shown in Table 9. Obviously, the TOF$_{ini,1}$ for reaction Route-I and the TOF$_{ini,2}$ for reaction Route-II on HBeta-M are much higher than those on the NS-HMOR and HMont catalysts in the *N*-alkylation of *p*-

toluenesulfonamide with benzhydrol **1a** or dibenzhydryl ether **4a**. This is consistent with the reaction rate results mentioned above. When the TOFs were determined based on the strong acid sites in the mesoporous, the obtained initial turnover frequencies of $TOF^S_{ini,\,1}$ for reaction Route-I on the HBeta-M, HMont and NS-HMOR catalysts is 46.1, 38.9 and $7.7 \times 10^{-2}$ s$^{-1}$, respectively. This is in line with the order of the initial reaction rates on three catalysts for the Route-I. This could be due to the fact that HBeta-M has a large amount of strong acidic sites (as discussion in characterization section), which contributes to the high-efficiency in the *N*-alkylation of *p*-toluenesulfonamide with benzhydrol. In addition, we also compared the TOFs to relevant reactions reported in the literatures (Table S3). The HBeta-M catalyst has a higher TOF than the previously reported catalytic systems using homogeneous and heterogeneous noble metal catalysts.

**Table 9.** The reaction rates and turnover frequencies of the different catalysts in *N*-alkylation of *p*-toluenesulfonamide reaction.

| Catalyst | $r_{obs,1}{}^a$ (×10$^{-3}$ mol·kg$^{-1}$·s$^{-1}$) | $r_{obs,2}{}^b$ (×10$^{-3}$ mol·kg$^{-1}$·s$^{-1}$) | $TOF_{ini,1}{}^a$ (×10$^{-2}$ s$^{-1}$) | $TOF^S_{ini,1}{}^a$ (×10$^{-2}$ s$^{-1}$) | $TOF_{ini,2}{}^b$ (×10$^{-2}$ s$^{-1}$) |
|---|---|---|---|---|---|
| HBeta-M | 13 | 9.8 | 11.0 | 46.1 | 8.3 |
| NS-HMOR | 3.6 | 5.2 | 3.3 | 38.9 | 4.7 |
| HMont | 2.5 | 1.6 | 4.0 | 7.7 | 2.6 |

[a]Reaction condition: 0.1 g catalyst (120-140 mesh), 7.5 mmol benzhydrol **1a**, 15 mmol *p*-toluenesulfonamide **2a**, 130 mL DCE, 1.0 mL diphenylmethane, 80 °C, 500 rpm.

[b]Reaction condition: 0.1 g catalyst (120-140 mesh), 3.75 mmol dibenzhydryl ether **4a**, 15 mmol *p*-toluenesulfonamide **2a**, 130 mL DCE, 1.0 mL diphenylmethane, 80 °C, 500 rpm.

On the other hand, the evolution of the dibenzhydryl ether **4a** selectivity with reaction time on the three catalysts is presented in Figure 10. For comparison, the selectivity of the product **3a** was also presented in the Figure 10. For the HBeta-M catalyst, the dibenzhydryl ether **4a** selectivity is slightly higher than product **3a** selectivity at the initial reaction stage, while dibenzhydryl ether **4a** selectivity decreases gradually and product **3a** selectivity increases with prolongation of the reaction time. When the reaction time reached to 9 h, the product **3a** selectivity is higher than **4a** selectivity on the HBeta-M catalyst (Figure 10a). For NS-HMOR and HMont catalysts, similar results were also obtained (Figure 10b and 10c). These results further demonstrate that at the initial reaction stage, benzhydrol **1a** was easily transformed into dibenzhydryl ether **4a** on the acidic catalyst, and with the prolongation of the reaction time, besides the benzhydrol **1a**, the dibenzhydryl ether **4a** can react with *p*-toluenesulfonamideto form the final product **3a**.
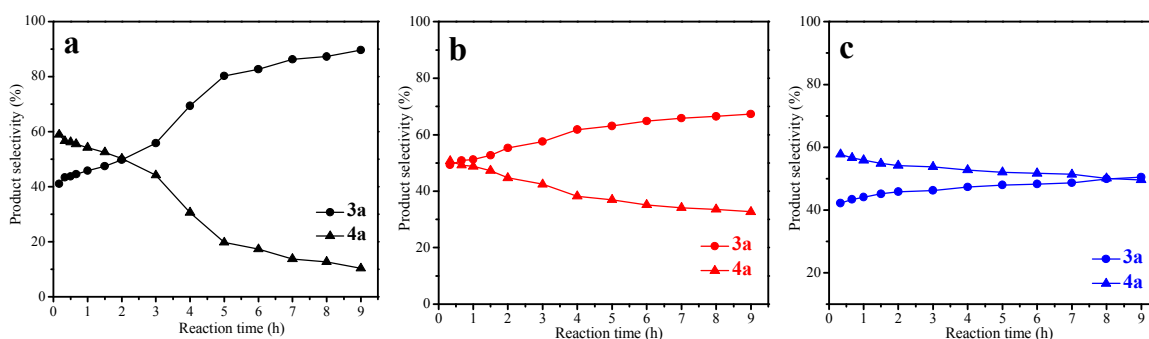


**Figure 10.** Dependence of the product selectivities of the **3a** and **4a** on the reaction time over the (a) HBeta-M, (b) NS-HMOR and (c) HMont catalysts in the 300 mL Parr autoclave.

### 3.3.4 High activity reason of HBeta-M catalyst

The high catalytic activity of HBeta-M can be attributed to not only the presence of abundant mesoporous channels, but also the existence of acid sites on HBeta-M, especially strong acid sites. The acid sites on the catalyst could benefit the adsorption and activation of the reactant

molecules, resulting in the formation of key intermediates. To verify this conclusion, the experiment for the adsorption of benzhydrol **1a** and dibenzhydryl ether **4a** on catalysts was preferentially performed, and the results are presented in Table 10. Obviously, the adsorption capacities of benzhydrol **1a** and dibenzhydryl ether **4a** on HBeta-M (52 and 90 mg·$g_{cat.}^{-1}$) are much higher than those on NS-HMOR (31 and 52 mg·$g_{cat.}^{-1}$) and HMont (19 and 43 mg·$g_{cat.}^{-1}$). The high adsorption capability of the substrates on the HBeta-M could be due to the abundant acidic sites on the HBeta-M. In this case, the adsorbed substrates can be interacted with Brönsted acidic sites ($H^+$) to form key intermediates. Figure 11 and Figure 12 show the UV-Vis DR and IR spectra of benzhydrol **1a** and dibenzhydryl ether **4a** chemisorbed on HBeta-M (HBeta-M-**1a**, HBeta-M-**4a**) and HMont (HMont-**1a**, HMont-**4a**), respectively.

**Table 10.** The adsorption capacity of the benzhydrol **1a** and dibenzhydryl ether **4a** on the HBeta-M, NS-HMOR and HMont catalysts.

| Catalyst | Adsorption capacity (mg·$g_{cat.}^{-1}$) | |
| --- | --- | --- |
| | Benzhydrol **1a** | Dibenzhydryl ether **4a** |
| HBeta-M | 52 | 90 |
| NS-HMOR | 31 | 52 |
| HMont | 19 | 43 |
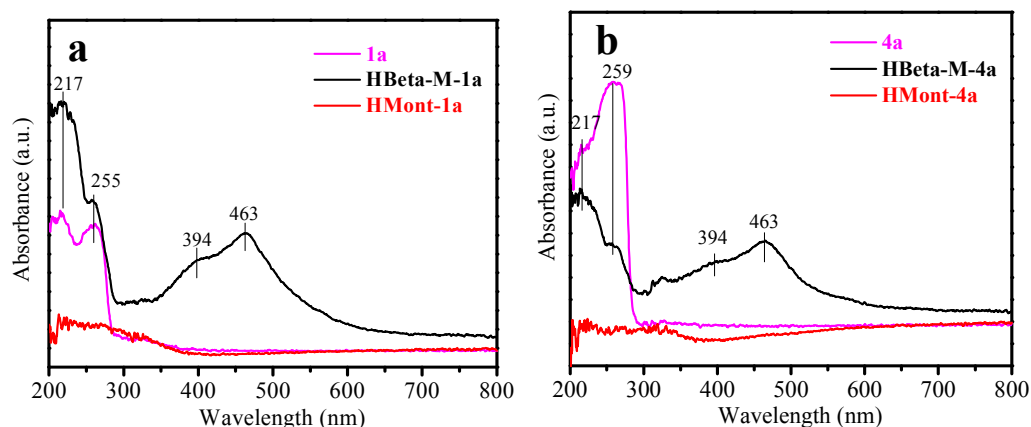
**Figure 11.** (a) UV-Vis DR spectra of pure **1a**, HBeta-M-**1a** and HMont-**1a**, and (b) UV-Vis DR spectra of pure **4a**, HBeta-M-**4a** and HMont-**4a**.
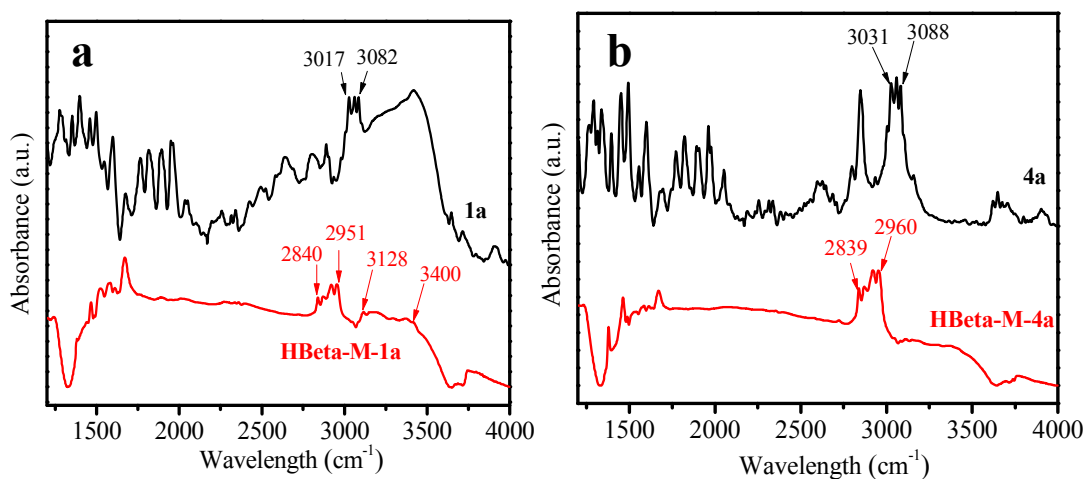


**Figure 12.** (a) IR spectra of pure **1a** and HBeta-M-**1a**, and (b) IR spectra of pure **4a** and HBeta-M-**4a**.

From Figure 11a, the UV-Vis DR spectrum of pure benzhydrol **1a** shows two absorption bands at 217 nm and 255 nm associated with the characteristics of the conjugate $\pi$ band in benzhydrol.[26] As comparison, for the HBeta-M-**1a** sample, in addition to the two bands at 217 and 255 nm, a broad absorption band centered at 463 nm is observed with a shoulder at 394 nm in the HBeta-M-**1a** sample, which could result from the formation of a benzhydryl carbocation.[42]

In contrast, the HMont-**1a** sample only shows a very weak absorption band at approximately 255 nm (Figure 11a). These results indicate that the adsorbed benzhydrol **1a** molecule on HBeta-M can interact readily with the acid sites ($H^+$) to form oxonium ions intermediate, and subsequently undergo loss of water to form benzhydryl carbocation. Similarly, the UV-Vis DR spectrum of the HBeta-M-**4a** sample shows four absorption bands at 217, 259, 394 and 463 nm (Figure 11b), which indicates that benzhydryl carbocation could also be formed after **4a** adsorbed on the HBeta-M. These conclusions were further confirmed by the IR analysis of the HBeta-M-**1a** and HBeta-M-**4a** samples, and the results are shown in Figure 12.

Figure 12a show the absorption bands in the range 3017-3082 $cm^{-1}$ for the C-H stretching vibration of pure benzhydrol **1a**,[43] which shift to lower frequencies in the range of 2840-2951 $cm^{-1}$ for the HBeta-M-**1a** sample. This can be explained that an empty *p*-orbital in the formed carbocation could be conjugated with the $\pi$-system of the benzene ring, which would result in extensive delocalization of the charge from the phenyl rings. As a result, the electron density of the $\pi$-conjugated system would decrease, leading to the redshift. A similar redshift phenomenon was also observed in the IR spectrum of the HBeta-M-**4a** sample (Figure 12b). Additionally, a broad absorption band in the range of 3128-3400 $cm^{-1}$ was observed for the HBeta-M-**1a** sample (Figure 12a), which could be assigned to the presence of associated hydrogen bond and formation of associated benzhydrol when benzhydrol **1a** adsorbed on HBeta-M sample. This broad absorption band related to the associated hydrogen bond was also observed on the HBeta-M-**4a** sample (Figure 12b). This result indicates that after the **4a** chemisorbed on HBeta-M, the associated benzhydrol **1a** could be formed. Combining the results from the UV-Vis and IR analyses, it can be concluded that the HBeta-M sample with strong acid sites could activate the adsorbed **1a** and **4a** molecules, leading to the formation of carbocation intermediates.

Additionally, besides the acidity of the catalyst, the presence of mesoporous structure in the HBeta-M also plays an important role for improving the reaction activity. The HBeta-M has meso- and micro-pores structure, and the mesopores are interconnected micropores (Figure S10). The micropore mouth is open up on the mesopore surface, in this manner, the micropore openings can provide abundant acidic sites for mesopore surface. When the bulky reactant molecules diffused into the mesopores channels, the reactant could be accessible the acidic sites in the micropore openings. Because the reactant and the target product have large molecular dimension (Table S1), the reaction mainly occurs in the mesoporous channels and on the outer surface of the catalysts. HBeta-M has large mesoporous surface area (180 $m^2 \cdot g^{-1}$) and mesoporous volume (0.27 $cm^3 \cdot g^{-1}$), while HBeta presents low external surface area (58 $m^2 \cdot g^{-1}$). The abundant mesopores in HBeta-M can favor the diffusion of reactants and products with large molecular dimension. As a result, the activity of HBeta-M is higher than that of HBeta.

### 3.3.5 Reaction mechanism on HBeta-M catalyst

Basing on the experiment and characterization results discussed above, the reaction mechanism of the *N*-alkylation reaction on the HBeta-M catalyst is shown in Figure 13. Benzhydrol **1a** can be chemisorbed on the acidic sites and protonated by $H^+$ to give benzhydryloxonium **5**. Subsequent dehydration of **5** results in the formation of the carbocation **6**. Simultaneously, benzhydrol **1a** is also easily converted to dibenzhydryl ether **4a** with the help of the $H^+$ in zeolite HBeta-M, which is followed by protonation on the acidic sites to give intermediate **7**. Elimination of one benzhydrol from intermediate **7** occurs and forms carbocation **6**. Finally, Carbocation **6** is attacked by the electric-rich sulfonamide nucleophile, followed by elimination of a proton to generate the final target *N*-substituted sulfonamide product **3a**.
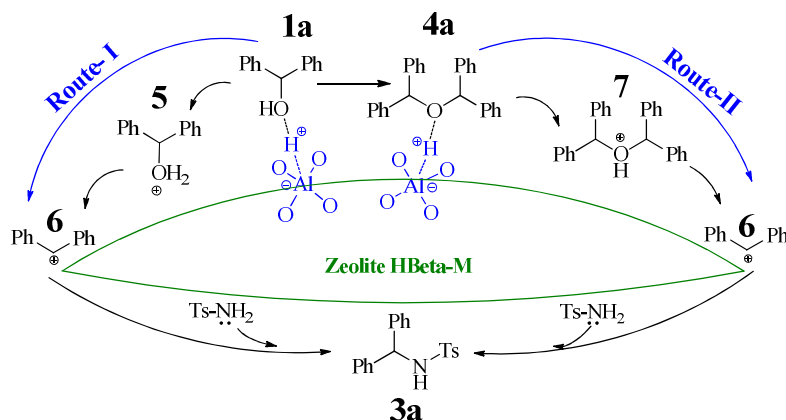
**Figure 13**. Reaction mechanism of the direct *N*-alkylation of sulfonamides with benzhydrols on HBeta-M.

## 3.4 Recycling ability of HBeta-M catalyst

The recycle performance of the HBeta-M catalyst was also surveyed. HBeta-M exhibits good catalytic activity and product selectivity after four cycles (Table S4). The XRD pattern of the reused HBeta-M catalyst shows the same diffraction peak location as to the fresh catalyst (Figure S11). In addition, the textural parameters and the $NH_3$-TPD curve of the recovered catalyst are similar to those of the fresh one (Table 1 and Figure S12). These results indicate that the physical-chemical properties of the recycled catalyst are maintained well.

## 4 Conclusions

The reaction route and mechanism of the direct *N*-alkylation of *p*-toluenesulfonamide sulfonamide with benzhydrol on acidic mesoporous zeolite Beta catalysts (HBeta-M) were investigated in detail. There are two parallel reaction routes present on the acidic catalysts, demonstrated by experiment results. The reaction Route-I is that the benzhydrol can be activated on Brönsted acidic sites ($H^+$) to form an intermediate of benzhydryloxonium that further transforms to carbocation, which reacts with sulfonamide to form final product *N*-benzhydryl-4-

methylbenzenesulfonamide. Another reaction Route-II is first found in this work. The benzhydrol also can be converted to dibenzhydryl ether on the acidic sites, and subsequently, the dibenzhydryl ether is catalyzed by acidic sites to form corresponding oxonium, which further transforms to carbocation. The carbocation is attacked by the electric-rich sulfonamide nucleophile to generate the final product. In addition, the reaction Route-II predominantly contributes to the formation of the target product with high selectivity on the acidic catalysts. The strong acidic sites on HBeta-M facilitate the enhancement of the reaction rate. The mesoporous in the HBeta-M improve the mass transfer and further benefit this transformation.

ASSOCIATED CONTENT

**Supporting Information**. The Supporting Information is available free of charge on the ACS Publications website at http://pubs.acs.org.

Table S1−S4 and Figures S1−S12 as described in the text (PDF).

AUTHOR INFORMATION

**Corresponding Author**

*E-mail for Q.C.: chenqunjpu@yahoo.com

*E-mail for A. Z.:zhenganm@wipm.ac.cn

*E-mail for T.T.: tangtiandi@cczu.edu.cn

**Author Contributions**

Tiandi Tang and Qun Chen proposed the research direction and guided the project. Tiandi Tang and Anming Zheng designed the experiments. Wenqian Fu and Runsheng Shen synthesized the zeolites and performed the *N*-alkylation reaction. Enhui Bai and Zhongxue Fang performed the experiment of substrate scope. Guangchao Li, Xianfeng Yi and Anmin Zheng performed the ^{31}P NMR experiment and analysis the result. Wenqian Fu, Lei Zhang and Tiandi Tang analyzed and discussed the experimental results and drafted the manuscript.

**Notes**

The authors declare no competingfinancial interest.

REFERENCES

(1) Das, B. G.; Nallagonda, R.; Ghorai, P. Direct substitution of Hydroxy Group of π-Activated Alcohols with Electron-Deficient Amines Using $Re_2O_7$ Catalyst. *J. Org. Chem.* 2012, 77, 5577-5583.

(2) Fan, X.; Fu L.-A.; Li, N.; Lv, H.; Cui, X.-M.; Qi, Y. Iron-Catalyzed *N*-Alkylation Using π-Activated Ethers as Electrophiles. *Org. Biomol. Chem.* 2013, 11, 2147-2153.

(3) Yang, Q.; Wang, Q.; Yu, Z. Substitution of Alcohols by *n*-Nucleophiles via Transition Metal-Catalyzed Dehydrogenation. *Chem. Soc. Rev.* 2015, 44, 2305-2329.

(4) Reddy, C. R.; Madhavi, P. P.; Reddy, A. S. Molybdenum(V) Chloride-Catalyzed Amidation of Secondary Benzyl Alcohols with Sulfonamides and Carbamates. *Tetrahedron Lett.* 2007, 48, 7169-7172.

(5) Zhu, A.; Li, L.; Wang, J.; Zhuo K. Direct Nucleophilic Substitution Reaction of Alcohols Mediated by a Zinc-Based Ionic Liquid. *Green Chem.* 2011, 13, 1244-1250.

(6) Di Gioia, M. L.; Leggio, A.; Liguori, A.; Perri, F. Solid-Phase Synthesis of *N*-Nosyl- and *N*-Fmoc-*N*-Methyl-α-amino Acids. *J. Org. Chem.* 2007, 72, 3723-3728.

(7) Kan, T.; Fukuyama, T. Ns Strategies: a Highly Versatile Synthetic Method for Amines. *Chem. Commun.* 2004, 0, 353-359.

(8) Abdel-Magid, A. F.; Mehrman, S. J. A Review on the Use of Sodium Triacetoxyborohydride in the Reductive Amination of Ketones and Aldehydes. *Org. Process Res. Dev* 2006, 10, 971-1031.

(9) Yamaguchi, R.; Kawagoe, S.; Asai, C.; Fujita, K.-i. Selective Synthesis of Secondary and Tertiary Amines by Cp*Iridium-Catalyzed Multialkylation of Ammonium Salts with Alcohols. *Org. Lett.* 2008, 10, 181-184.

(10) Shi, F.; Tse, M. K.; Zhou, S.; PohI, M.-M.; Radnik, J.; Hübner, S.; Jähnisch, K.; Brückner, A.; Beller M. Green and Efficient Synthesis of Sulfonamides Catalyzed by Nano-Ru/Fe$_3$O$_4$. *J. Am. Chem. Soc.* 2009, 131, 1775-1779.

(11) Qin, H.; Yamagiwa, N.; Matsunaga, S.; Shibasaki, M. Bismuth-Catalyzed Direct Substitution of the Hydroxy Group in Alcohols with Sulfonamides, Carbamates, and Carboxamides. *Angew. Chem., Int. Ed.* 2007, 119, 413-417.

(12) Zhan, Z.-P.; Yang, W.-Z.; Yang, R.-F.; Yu, J.-L.; Li, J.-P.; Liu, H.-J. BiCl$_3$-Catalyzed Propargylic Substitution Reaction of Propargylic Alcohols with C-, O-, S- and N-centered Nucleophiles. *Chem. Commun.* 2006, 31, 3352-3354.

(13) Shi, F.; Tse, M. K.; Cui, X.; Gördes, D.; Michalik, D.; Thurow, K.; Deng, Y.; Beller, M. Copper-Catalyzed Alkylation of Sulfonamides with Alcohols. *Angew. Chem.* 2009, 121, 6026-6029.

(14) Corma, A.; Navas, J.; Sabater, M. Advances in One-Pot Synthesis through Borrowing Hydrogen Catalysis. *J. Chem. Rev.* 2018, 118, 1410-1459.

(15) Wang, G.-W.; Shen, Y.-B.; Wu, X.-L. Phosphotungstic Acid Catalyzed Amidation of Alcohols. *Eur. J. Org. Chem.* 2008, 25, 4367-4371.

(16) Motokura, K.; Nakagiri N.,; Mori K.; Mizugaki, T.; Ebitani, K.; Jitsukawa K.; Kaneda K. Efficient C-N Bond Formations Catalyzed by a Proton-Exchanged Montmorillonite as a Heterogeneous Brønsted Acid. *Org. Lett.* 2006, 8, 4617-4620.

(17) Motokura, K.; Nakagiri, N.; Mizugaki, T.; Ebitani, K.; Kaneda, K. Nucleophilic Substitution Reactions of Alcohols with Use of Montmorillonite Catalysts as Solid Brønsted Acids. *J. Org. Chem.* 2007, 72, 6006-6015.

(18) Qureshi, Z. S.; Deshmukh, K. M.; Tambade, P. J.; Dhake, K. P.; Bhanage, B. M. Amberlyst-15 in Ionic Liquid: An Efficient and Recyclable Reagent for Nucleophilic Substitution of Alcohols and Hydroamination of Alkenes. *Eur. J. Org. Chem.* 2010, 32, 6233-6238.

(19) Reddy, M. M.; Kumar, M. A.; Swamy, P.; Naresh, M.; Srujana, K.; Satyanarayana, L.; Venugopala A.; Narender, N. *N*-Alkylation of Amines with Alcohols over Nanosized Zeolite Beta. *Green Chem.* 2013, 15, 3474-3483.

(20) Vázquez, P.; Pizzio, L.; Cáceres, C.; Blanco, M.; Thomas, H.; Alesso, E.; Finkielsztein. L.; Lantaño, B.; Moltrasio, G.; Aguirre, J. Silica-Supported Heteropolyacids as Catalysts in Alcohol Dehydration Reactions. *J. Mole. Catal., A* 2000, 161, 223-232.

(21) Dusselier, M.; Deimund, M. A.; Schmidt, J. E.; Davis, M. E. Methanol-to-Olefins Catalysis with Hydrothermally Treated Zeolite SSZ-39. *ACS Catal.* 2015, 5, 6078-6085.

(22) Zhu, X.; Hofmann, J. P.; Mezari, B.; Kosinov, N.; Wu, L.; Qian, Q.; Weckhuysen, B. M.; Asahina, S.; Ruiz-Martínez, J.; Hensen, E. J. M. Trimodal Porous Hierarchical SSZ-13 Zeolite with Improved Catalytic Performance in the Methanol-to-Olefins Reaction. *ACS Catal.* 2016, 6, 2163-2177.

(23) Zhang L.; Fu W.; Yu, Q.; Tang, T.; Zhao, Y.; Li, Y. Effect of Citric Acid Addition on the Morphology and Activity of $Ni_2P$ Supported on Mesoporous Zeolite ZSM-5 for the Hydrogenation of 4,6-DMDBT and Phenanthrene. *J. Catal.* 2017, 345, 295-307.

(24) Fu, W.; Feng, Y.; Fang, Z.; Chen, Q.; Tang, T.; Yu, Q.; Tang, T. Zeolite Y Nanosheet Assembled Palladium Catalysts with High Catalytic Activity and Selectivity in the Vinylation of Thiophenes. *Chem. Commun.* 2016, 52, 3115-3118.

(25) Zheng, X.; Fu, W.; Xiong, J.; Xi, J.; Ni, X.; Tang, T. Zeolite Beta Nanoparticles Assembled Cu Catalysts with Superior Catalytic Performances in the Synthesis of Thioesters by Cross-Coupling of Aldehydes and Disulfides. *Catal. Today* 2016, 264, 152-157.

(26) Chen, S.; Shao, Z.; Fang, Z.; Chen, Q.; Tang, T.; Fu, W.; Zhang, L.; Tang, T. Design and Synthesis of the Basic Cu-Doped Zeolite X Catalyst with High Activity in Oxidative Coupling Reactions. *J. Catal.* 2016, 338, 38-46.

(27) Zhang, L.; Fu, W.; Yu, Q.; Tang, T.; Zhao, Y.; Zhao, H.; Li, Y. $Ni_2P$ Clusters on Zeolite Nanosheet Assemblies with High Activity and Good Stability in the Hydrodesulfurization of 4,6-Dimethyldibenzothiophene. *J. Catal.* 2016, 338, 210-221.

(28) Wang, C.; Liu, Z.; Wang, L.; Dong, X.; Zhang, J.; Wang, G.; Han, S.; Meng, X.; Zheng, A.; Xiao, F. Importance of Zeolite Wettability for Selective Hydrogenation of Furfural over Pd@Zeolite Catalysts. *ACS Catal.* 2018, 8, 474-481.

(29) Ramos Pinto, R.; Borges, P.; Lemos, M.A.N.D.A.; Lemos, F.; Védrine, J.C.; Derouane, E.G.; Ramôa Ribeiro, F. Correlating $NH_3$-TPD and ^{1}H MAS NMR Measurements of Zeolite Acidity: Proposal of an Acidity Scale. *Appl. Catal. A.: Gen.* 2005, 284, 39-46.

(30) Costa C.; Lopes, J.M.; Lemos, F.; Ramôa Ribeiro, F. Acidity-Activity Relationship in Zeolite Y. A Preliminary Study for *N*-Heptane Transformation. *Catal. Lett.* 1997, 44, 255-257.

(31) Badoga, S.; Dalai, A. K.; Adjaye, J.; Hu, Y. Combined Effects of EDTA and Heteroatoms (Ti, Zr, and Al) on Catalytic Activity of SBA-15 Supported NiMo Catalyst for Hydrotreating of Heavy Gas Oil. *Ind. Eng. Chem. Res.* 2014, 53, 2137-2156.

(32) Liu, L.; Wang, B.; Du, Y.; Zhong, Z.; Borgna, A. Bifunctional $Mo_3VO_x/H_4SiW_{12}O_{40}/Al_2O_3$ Catalysts for One-Step Conversion of Glycerol to Acrylic Acid: Catalyst Structural Evolution and Reaction Pathways. *Appl. Catal., B* 2015, 174-175, 1-12.

(33) Li, X.; Zheng, W. L.; Pan, H.; Yu, Y.; Chen, L.; Wu, P. Pt Nanoparticles Supported on Highly Dispersed $TiO_2$ Coated on SBA-15 as an Efficient and Recyclable Catalyst for Liquid-Phase Hydrogenation. *J. Catal.* 2013, 300, 9-19.

(34) Díaz-Rey, R. M.; Paris, C.; Martínez-Franco, R.; Moliner, M.; Martínez, C.; Corma, A. Efficient Oligomerization of Pentene into Liquid Fuels on Nanocrystalline Beta Zeolites. *ACS Catal.* 2017, 7, 6170-6178.

(35) Zheng, A.; Liu, S.-B.; Deng, F. ^{31}P NMR Chemical Shifts of Phosphorus Probes as Reliable and Practical Acidity Scales for Solid and Liquid Catalysts. *Chem. Rev.* 2017, 117, 12475–12531.

(36) Zheng, A.; Huang, S.-J.; Chen, W.-H.; Wu, P.-H.; Zhang, H.; Lee, H.-K.; de Ménorval, L.-C.; Deng, F.; Liu, S.-B. [31]P Chemical Shift of Adsorbed Trialkylphosphine Oxides for Acidity Characterization of Solid Acids Catalysts. *J. Phys. Chem. A* 2008, 112, 7349-7356.

(37) G.-Marek, K.; Tarach, K.; Choi, M. 2,6-Di-tert-butylpyridine Sorption Approach to Quantify the External Acidity in Hierarchical Zeolites. *J. Phys. Chem. C* 2014, 118, 12266-12274.

(38) Bui, P. P.; Oyama, S. T.; Takagaki, A.; Carrow, B. P.; Nozaki, K. Reactions of 2-Methyltetrahydropyran on Silica-Supported Nickel Phosphide in Comparison with 2-Methyltetrahydrofuran. *ACS Catal.* 2016, 6, 4549-4558.

(39) Alharbi, K.; Alharbi, W.; Kozhevnikova, E. F.; Kozhevnikov, I. V. Deoxygenation of Ethers and Esters over Bifunctional Pt-Heteropoly Acid Catalyst in the Gas Phase. *ACS Catal.* 2016, 6, 2067-2075.

(40) Hanna, D. G.; Shylesh, S.; Werner, S.; Bell, A. T. The Kinetics of Gas-Phase Propene Hydroformylation over a Supported Ionic Liquid-Phase (SILP) Rhodium Catalyst. *J. Catal.* 2012, 292, 166-172.

(41) Hoesterey, B.; Neely, W. C.; Worley, S. D. A Semi-Empirical MO Study of a Series of Amide, Imidic Acid, and Imidate Isomers. *Chem. Phys. Lett.* 1983, 94, 311-315.

(42) Rathore, R.; Burns, C. L.; Guzei, I. A. Synthesis and Isolation of Polytrityl Cations by Utilizing Hexaphenylbenzene and Tetraphenylmethane Scaffolds. *J. Org. Chem.* 2004, 69, 1524-1530.

(43) Desai, N. C.; Bhatt, N.; Somani, H.; Trivedi, A. Synthesis, Antimicrobial and Cytotoxic Activities of Some Novel Thiazole Clubbed 1,3,4-Oxadiazoles. *Eur. J. Med. Chem.* 2013, 67, 54-59.

**Table of Contents graphic**



Two parallel reaction routes for the direct *N*-alkylation of sulfonamides with alcohols over the acidic catalyst